Supporting Information

Highly efficient and stable hybrid quantum-dot light-emitting field-effect transistors

Penghui He, Linfeng Lan*, Caihao Deng, Jian Wang, Junbiao Peng, and Yong Cao

State Key Laboratory of Luminescent Materials and Devices, South China University of Technology, Guangzhou 510640, China.

E-mail: lanlinfeng@scut.edu.cn

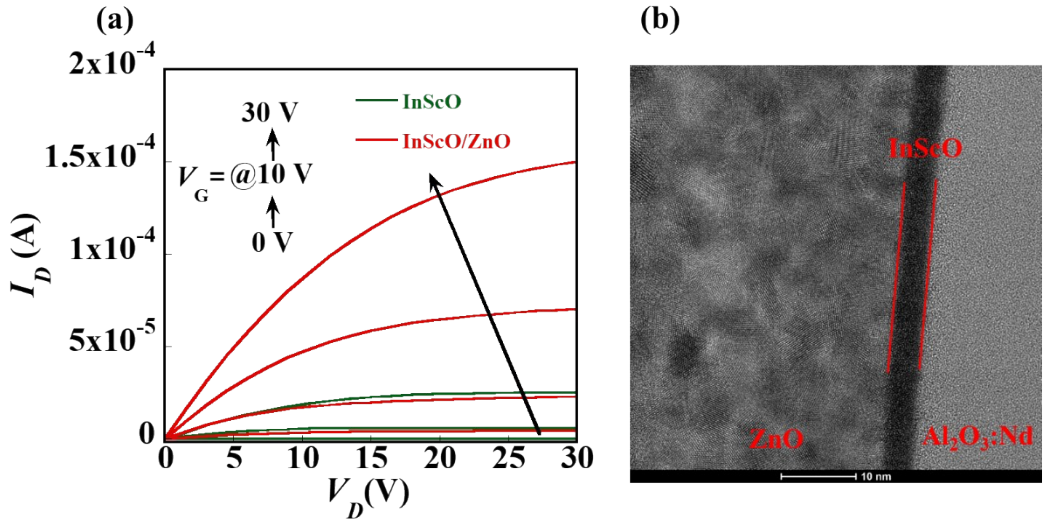

Figure S1. a The output curves of the TFTs with the channel layer of InScO and InScO/ZnO; b The TEM image of the TFT with the channel layer of InScO/ZnO.

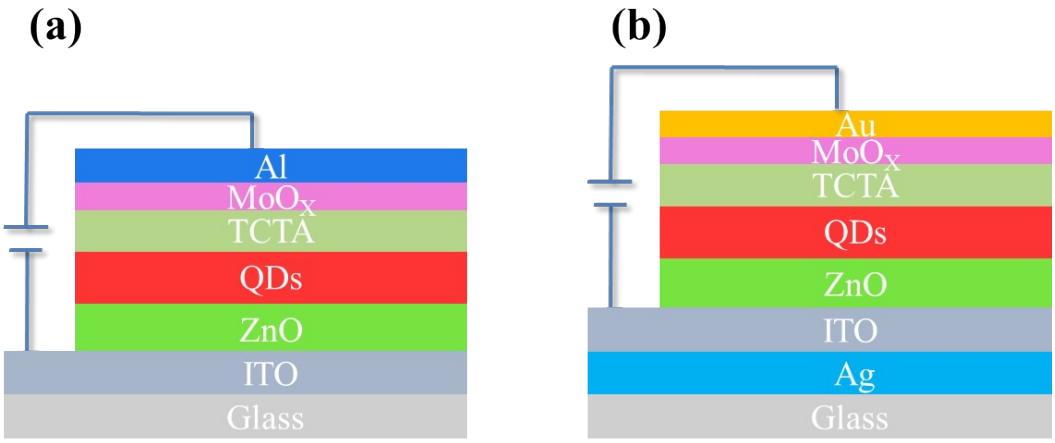

Figure S2. a The schematic structure of the bottom-emitting QLED. **b** The schematic structure of the equivalent top-emitting QLED.

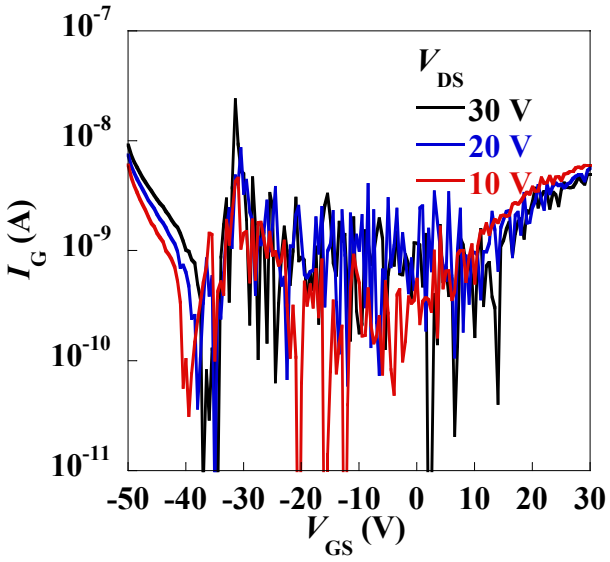

Figure S3. The gate leakage current (I_G) recorded simultaneously during the transfer characteristic (I_{DS} VS V_{GS}) measurements of the QD-HLET.

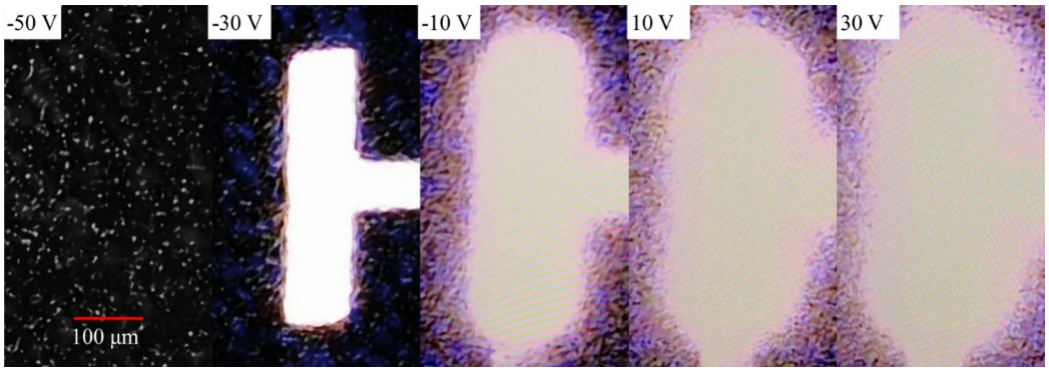

Figure S4. Microscopic images of red QD-HLETs with a constant V_{DS} of 30 V and different V_{GS} of -50 V, -30 V, -10 V, 10 V, and 30 V.

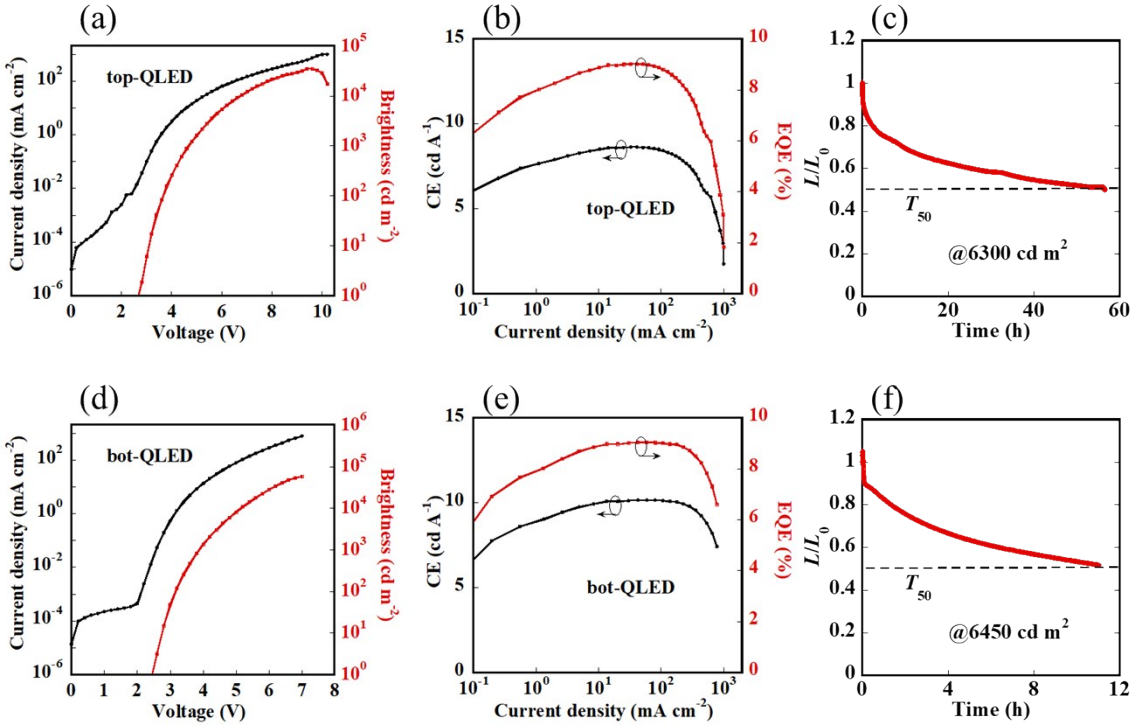

Figure S5. a Current density–luminance–voltage (*J-L-V*) curves of the equivalent top-emitting red QLED. **b** Current efficiency and EQE as functions of current density for the equivalent top-emitting red QLED with a structure of Ag(200 nm)/ ITO(10 nm)/ZnO(38 nm)/QDs(25 nm)/TCTA(50 nm)/MoO_X(8 nm)/Au(20 nm). **c** The operating lifetime curves of the equivalent top-emitting red QLED at a constant current density of 71 mA cm^{-2}, corresponding to an initial luminance of 6300 cd m^{-2}. **d** Current density–luminance–voltage (*J-L-V*) curves, **e** Current efficiency and EQE as functions of current density, **f** operational lifetime curves (at a constant current density of 71 mA cm^{-2}, corresponding to an initial luminance of 6450 cd m^{-2}) of the equivalent bottom-emitting red QLED with a structure of / ITO(150 nm)/ZnO(38 nm)/QDs(25 nm)/TCTA(50 nm)/MoO_X(8 nm)/Al(120 nm).

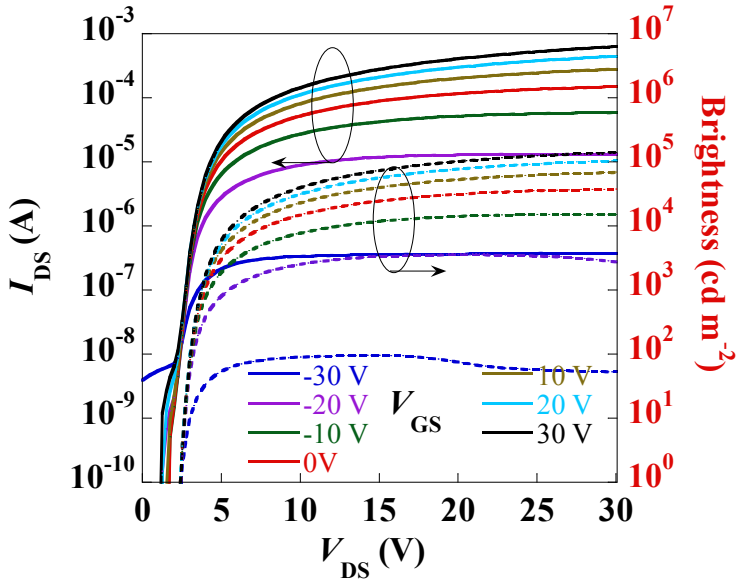

Figure S6. a The electronical and optical output characteristics of the red QD-HLET with a hole transport layer of TCTA.

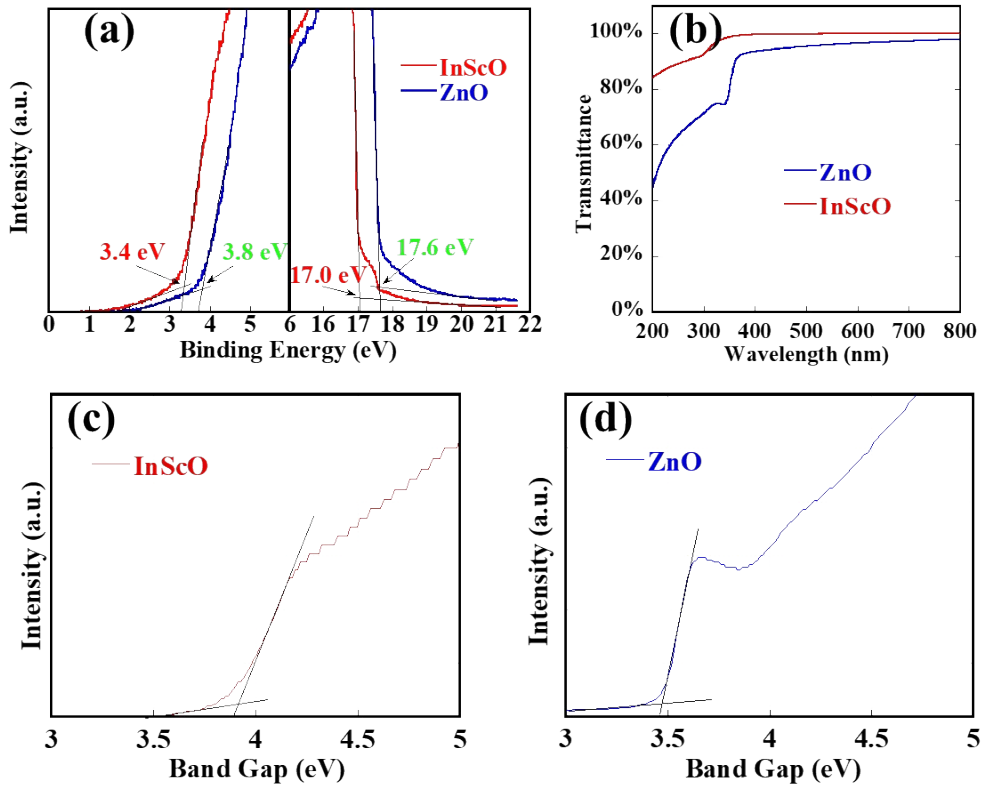

Figure S7. The UPS **a** and transmittance **b** of InScO and ZnO-nanoparticle. The $(\alpha h\upsilon)^2$ versus $h\upsilon$ curves of InScO **c** and ZnO **d**. The thickness of InScO and ZnO-nanoparticle is 3.4 nm and 38 nm, respectively.

The energy band levels of InScO and ZnO-nanoparticle films can be derived from the ultraviolet photoelectron spectroscopy (UPS) and UV-visible absorption spectroscopy measurements, as shown in Figure S7a, c and d, respectively. The optical bandgap (E_G^{OPT}) is calculated using Tauc analysis:[1]

$$\alpha h\upsilon = C(h\upsilon - E_G^{OPT})^b \quad (1)$$

where α is the optical absorbance of the material, $h\upsilon$ is the incident photon energy, C is a constant, and b is an exponent that depends on the nature of the semiconductor bandgap. Because InScO is a direct bandgap semiconductor (See Figure S8), b=1/2 is used. Figure S7c and d show the corresponding $(\alpha h\upsilon)^2$ *versus* $h\upsilon$ curves. The extracted

optical bandgaps are 3.91 and 3.47 eV InScO (3.4 nm) and ZnO-nanoparticle (38 nm), respectively. Considering Burstein-Moss shift,[2,3] which is usually attributed to occupation of the conduction band (inducing optical transitions at energies higher than the minimum-energy fundamental electronic gap), the fundamental electronic bandgap (E_G^F) is smaller than the optical bandgap, and the magnitude of the Burstein-Moss shift (ΔE_G^{BM}), under free-electron theory, is described as

$$\Delta E_G^{BM} = E_G^{OPT} - E_G^F = \frac{h^2}{2m^*}(3\pi^2 n_e)^{2/3} \quad (2)$$

where, m* is the effective mass of the electrons, and n_e is the electron density (9.2×10^{19} cm^{-3} for InScO and 2.0×10^{14} cm^{-3} for ZnO-nanoparticle). m* for InScO is calculated from first-principles calculations to be ~$0.2m_e$ (me is the Electron rest mass), as shown in Figure S8. From Eq. (2), ΔEGBM is calculated to be 0.37 and 0.01 eV (corresponding to EGF of 3.54 and 3.46 eV) for InScO and ZnO-nanoparticle, respectively. The valance band maximum (VBM) is derived from the UPS spectra to be 7.58 and 7.47 eV for InScO and ZnO-nanoparticle, respectively. Then, the conduction band minimum (CBM) is calculated to be 4.04 and 4.01 eV for InScO and ZnO-nanoparticle, respectively.

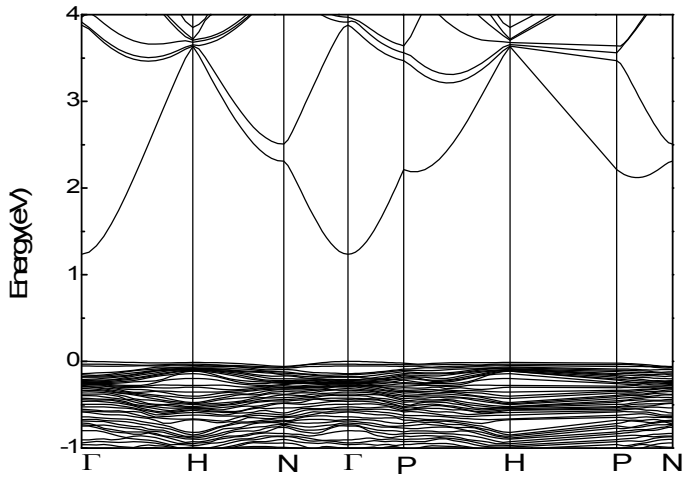

Direction	G-N	G-N	G-H
Effective mass at CBM (m^*/m_0)	0.1994	0.1975	0.2108

Figure S8. The calculated energy band structures and effective mass for InScO. The first-principles calculations were performed using the Vienna ab initio simulation package (VASP), where the projected augmented wave (PAW) method was adopted with the exchange-correlation functional in the form of Perdew-Burke-Ernzerhof (PBE). The atomic positions and cell parameters of candidates were fully relaxed until the energy differences were less than 0.001 eV. The cut-off energy of the plane wave was set to be 480 eV. The k meshes are distributed in reciprocal space with an average interval of 0.5$Å^{-1}$. With the structural recognition, we have excluded the duplicate configurations for the high-throughput screening with the first-principles calculations. We have adopted a supercell of In_2O_3 in bixbyite phase containing 32 In and 48 O atoms. Three Sc atoms have been doped into the supercell to replace In atoms, where 118 unique structures have been found for the first-principles

calculations.

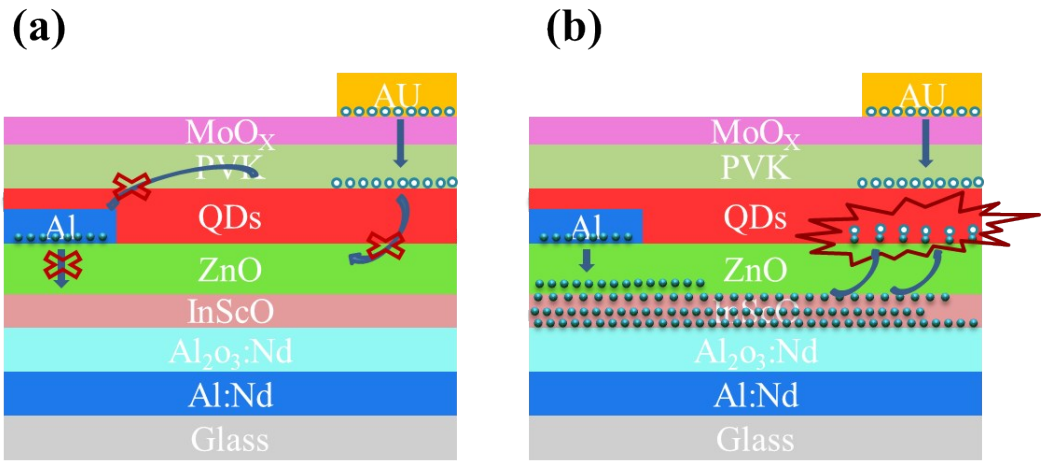

Figure S9. a The carrier distribution when the device is in off-state. **b** The carrier distribution when the device is in on-state.

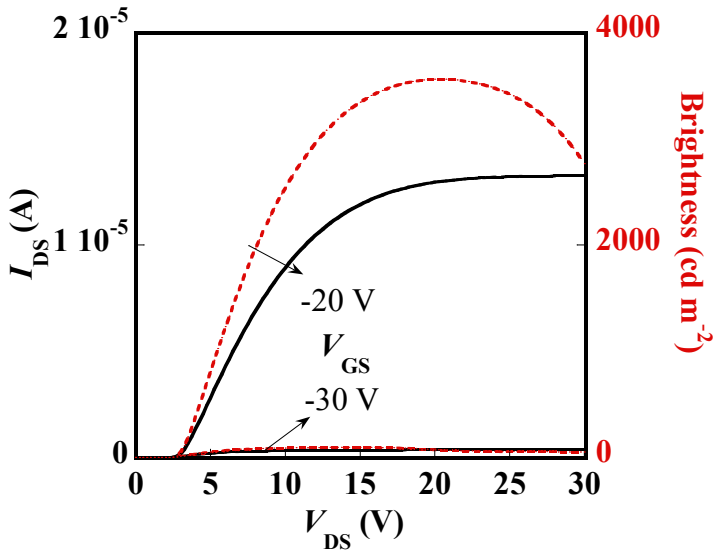

Figure S10. The electronical and optical output characteristics of the red QD-HLET at V_{GS} = -20 V and -30 V.

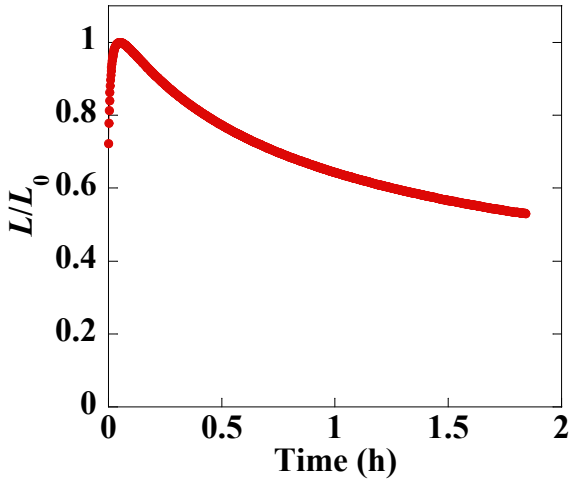

Figure S11. The operational lifetime of red QD-HLET without ZnO nanoparticle layer tested at constant current density of 71 mA cm^{-2}.

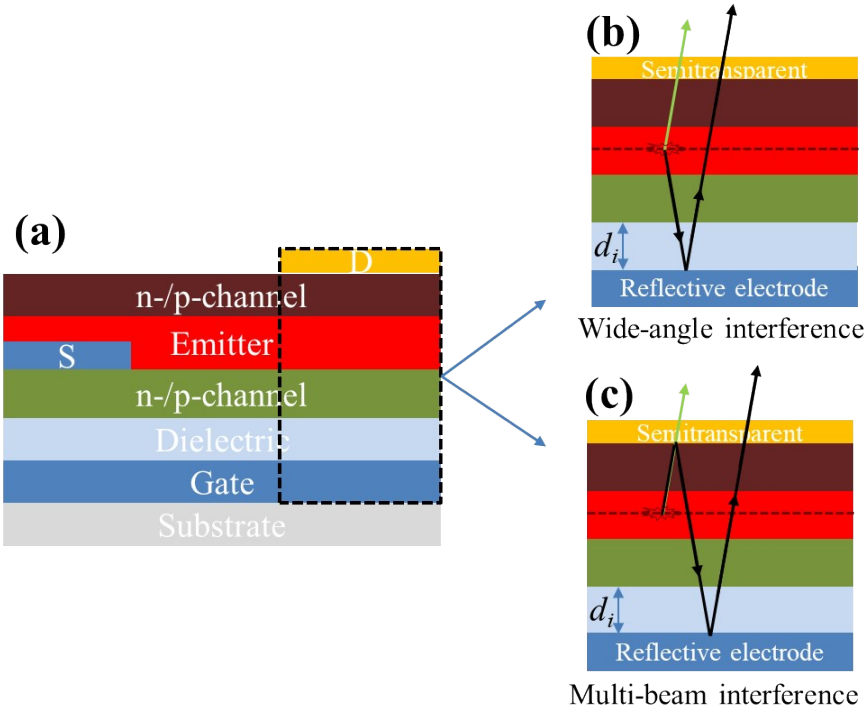

Figure S12. The device structure **a** wide-angle interference **b** and multiple-beam interference **c** of the QD-HLETs.

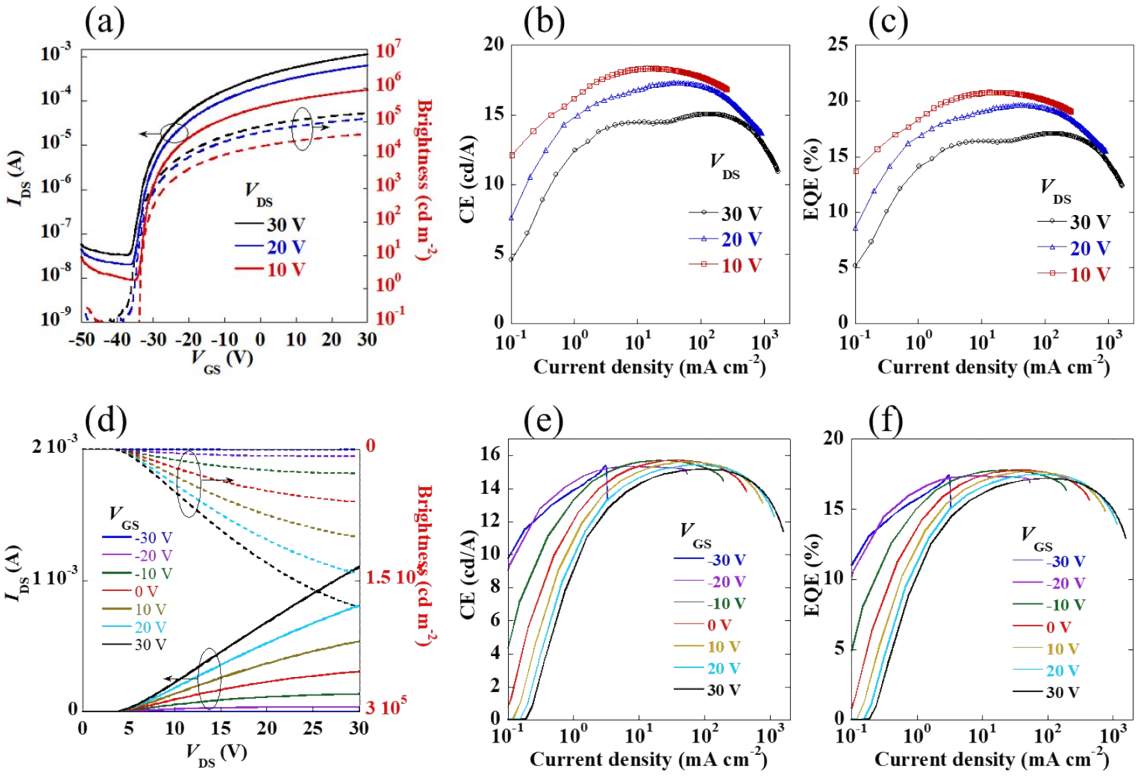

Figure S13. a The electrical and optical transfer characteristics curves, **b** current efficiency versus current density curves and **c**, EQE versus current density curves of red QD-HLET with 50 nm thick ZnO-nanoparticle (V_{DS} was held at different voltage of 10, 20, and 30 V, and V_{GS} swept from -50 to 30 V at each V_{DS}). **d** The electrical and optical output characteristics curves, **e** current efficiency versus current density curves and **f** corresponding EQE versus current density curves of Devices D (V_{GS} was held at different voltages between -20 to 30 V in step of 10 V, and V_{DS} swept from 0 to 30 V at each V_{GS}); the insets of (**e, f**) were the corresponding amplified curves.

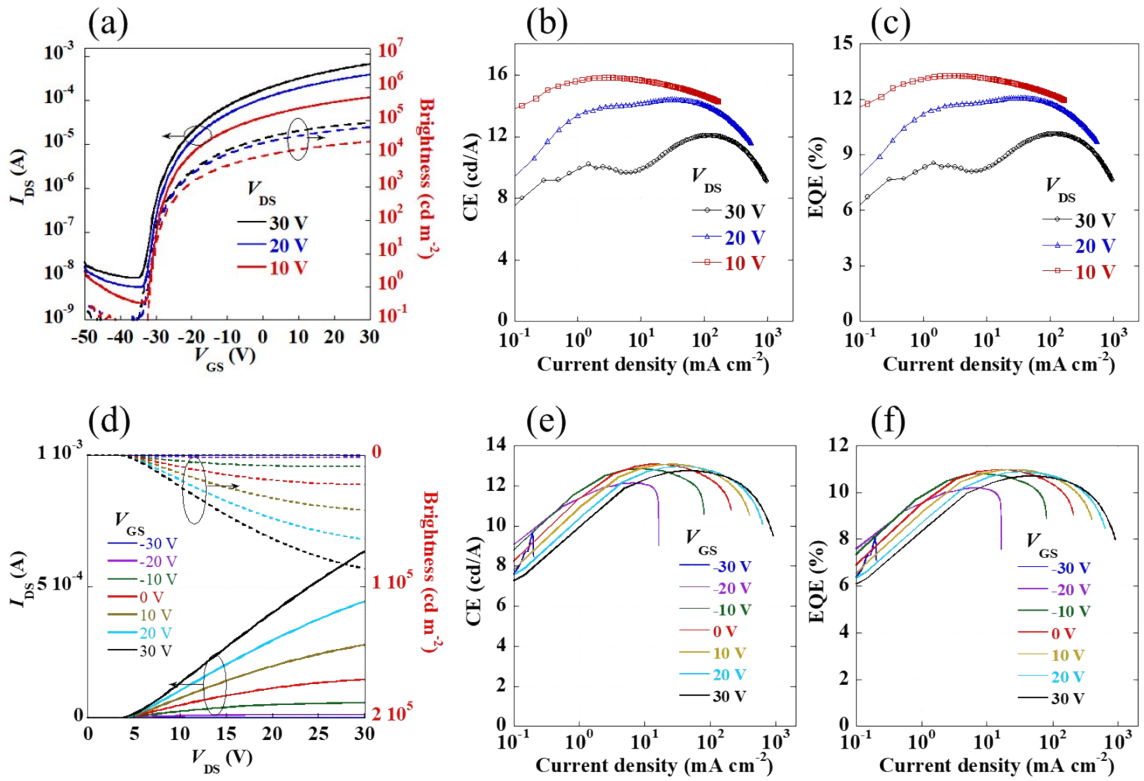

Figure S14. a The electrical and optical transfer characteristics curves, **b** current efficiency versus current density curves and **c**, EQE versus current density curves of red QD-HLET with 26 nm thick ZnO-nanoparticle (V_{DS} was held at different voltage of 10, 20, and 30 V, and V_{GS} swept from -50 to 30 V at each V_{DS}). **d** The electrical and optical output characteristics curves, **e** current efficiency versus current density curves and **f** corresponding EQE versus current density curves of Devices E (V_{GS} was held at different voltages between -20 to 30 V in step of 10 V, and V_{DS} swept from 0 to 30 V at each V_{GS}); the insets of (**e, f**) were the corresponding amplified curves.

Table S1. Comparison of electrical and optical properties of LETs in this work with others reported elsewhere.

Device types	Mobility ($cm^2 V^{-1} s^{-1}$)	EQE_{max} (%)	L_{max} (cd/m^2)	Current on/off ratio	T_{50} at 100 $cd\ m^{-2}$ (h)	Reference
Red-QDs	$_e$ 3.1	22.8	145000	~10^5	153000	This work
Red-QDs	$_e$ 0.8	8.7	13400	10^5	N/A	4
Green-QDs	$_e$ 25	11	8000	N/A	N/A	5
Perovskite	$_e$ 20	0.2	18	10^6	N/A	6
Alq_3:DCJTB	N/A	6.5	2190	N/A	N/A	7
NT4N	$_e$ 2.3×10^{-1} $_h$ 4.7×10^{-3}	N/A	1.7	N/A	N/A	8
Green-yellow	$_e$ 5	0.8	29000	10^6	N/A	9
TADF	$_h$ 0.11	3.76	1890	10^4	N/A	10
Super-yellow	$_e$ 1.2×10^{-1} $_h$ 3×10^{-3}	1.9	2100	1.7×10^5	N/A	11
F8BT	N/A	8.2	5500	<10^2	N/A	12
Alq_3:DCM	$_e$ 5×10^{-1} $_h$ 3×10^{-5}	5.5	N/A	<10^2	N/A	13

N/A, not available; $_e$, electron mobility; $_h$, hole mobility

Notes and References

S1 J. Tauc, R. Grigorovici, and A. Vancu, *Phys. Status Solidi* 1966, **15**, 627.

S2 T. S. Moss, *Proc. Phys. Soc., London, Sect.* B, 1954, **67**, 775.

S3 E. Burstein, *Phys. Rev.* 1954, **93**, 632.

S4 P. He, C. Jiang, L. Lan, S. Sun, Y. Li, P. Gao, P. Zhang, X. Dai, J. Wang, J. Peng, and Y. Cao, *ACS nano* 2018, **12**, 4624.

S5 X. Liu, W. Kuang, H. Ni, Z. Tao, J. Chang, Q. Liu, J. Ge, C. Li, and Q. Dai, *Small* 2018, **14**, 1800265.

S6 M. U. Chaudhry, N. Wang, K. Tetzner, A. Seitkhan, Y. Miao, Y. Sun, M. C. Petty, T. D. Anthopoulos, J. Wang, and D. D. C. Bradley, *Adv. Electron. Mater.* 2019, 1800985.

S7 J. Lee, T. Ke, J. Genoe, P. Heremans, and C. Rolin, *Adv. Electron. Mater.* 2019, **5**, 1800437.

S8 M. Natali, S. D. Quiroga, L. Passoni, L. Criante, E. Benvenuti, G. Bolognini, L. Favaretto, M. Melucci, M. Muccini, F. Scotognella, F. Di Fonzo, and S. Toffanin, *Adv. Funct. Mater.* 2017, **27**, 1605164.

S9 M. U. Chaudhry, K. Muhieddine, R. Wawrzinek, J. Li, S. Lo, and E. B. Namdas, *ACS Photonics* 2018, **5**, 2137.

S10 L. Song, Y. Hu, Z. Liu, Y. Lv, X. Guo, and X. Liu,*ACS Appl. Mater. Interfaces* 2017, **9**, 2711.

S11 M. Ullah, K. Tandy, S. D. Yambem, M. Aljada, P. L. Burn, P. Meredith, and E. B. Namdas, *Adv. Mater.* 2013, **25**, 6213.

S12 M. C. Gwinner, D. Kabra, M. Roberts, T. J. K. Brenner, B. H. Wallikewitz, C. R. McNeill, R. H. Friend, and H. Sirringhaus, *Adv. Mater.* 2012, **24**, 2728.

S13 R. Capelli, S. Toffanin, G. Generali, H. Usta, A. Facchetti, and M. Muccini, *Nat. Mater.* 2010, **9**, 496.